









Open Archive TOULOUSE Archive Ouverte (OATAO)

OATAO is an open access repository that collects the work of some Toulouse researchers and makes it freely available over the web where possible.

This is an author's version published in : <http://oatao.univ-toulouse.fr/19845>

Official URL : <https://dx.doi.org/10.1016/j.cep.2016.09.021>

To cite this version :

Lachin, Kevin  and Le Sauze, Nathalie  and Di Miceli Raimondi, Nathalie  and Aubin, Joelle  and Gourdon, Christophe  and Cabassud, Michel  *Aggregation and breakup of acrylic latex particles inside millimetric scale reactors*. (2017) *Chemical Engineering and Processing: Process Intensification*, vol. 113. pp. 65-73. ISSN 0255-2701

Any correspondence concerning this service should be sent to the repository administrator :
tech-oatao@listes-diff.inp-toulouse.fr

Aggregation and breakup of acrylic latex particles inside millimetric scale reactors

K. Lachin^{a,b}, N. Le Sauze^{a,b,*}, N. Di Miceli Raimondi^{a,b}, J. Aubin^{a,b}, C. Gourdon^{a,b}, M. Cabassud^{a,b}

^a Université de Toulouse, INPT, UPS, Laboratoire de Génie Chimique, 4 allée Emile Monso, F-31432 Toulouse Cedex 04, France

^b CNRS, Laboratoire de Génie chimique, F-31432 Toulouse Cedex 04, France

ARTICLE INFO

Keywords:

Latex coagulation
Millireactors
Aggregate breakup
Fractal dimension
Laminar flow

ABSTRACT

Aggregation of acrylic latex is investigated inside tubular millireactors working under laminar hydrodynamic conditions. The size distribution and fractal dimension of aggregates are measured using light scattering. Results show that the equilibrium between rupture and aggregation is achieved quickly, allowing the study of cluster size distribution and shape at the aggregation/rupture steady state. Both laminar hydrodynamic conditions and high shear rate are suspected to promote the formation of aggregates with a high fractal dimension, which means that the particles are almost spherical, thereby offering an interesting alternative to conventional batch processes. These results can provide useful information for industries aiming at producing aggregates at specified size and quality.

1. Introduction

Colloidal aggregation (or coagulation) is a common practice in a wide range of industries. In wastewater treatment, the role of aggregation/flocculation processes is to assist the removal of the undesired organic matter by forming strong aggregates from colloidal matter before separation [1]. Indeed, this phenomenon is of primary importance for the success of the water treatment process. In the polymer industries, latex coagulation, which typically occurs just after batch polymer synthesis, is a key process. It defines the size and shape of the final agglomerates and thus the properties of the resulting product. However, conventional coagulation techniques, which are typically performed in stirred tanks, can lead to quality and safety issues related to the size and shape of the clusters [2]. Understanding the fundamentals of colloidal coagulation and proposing new processes to perform the operation is thus essential for these industries.

Colloidal suspensions are metastable. The equilibrium between the attractive Van der Waals forces and the repulsive electrostatic forces, which are induced by the surface charges of the particles, grants interesting stability properties to these suspensions. As a result, they can spend extended periods of time without

deterioration or change in the particle size and associated properties. Due to the metastability of such suspensions, coagulation does not occur naturally for most cases and therefore must be triggered by a coagulant (acid or salt). When a salt is used, the coagulant lowers the repulsive forces by screening the charge effects. If the charged functions are pH sensitive, an acid can be used to change the pH of the medium and thus the charges at the surface of the colloidal particles.

The collision mode of the particles also plays an important role in coagulation. When the initial particles – or early clusters – are small enough (i.e. with diameters less than several hundred nanometers), Brownian motion causes the particles/clusters to move around their equilibrium position and temperature has an impact on the coagulation rate. In such cases, the term perikinetic coagulation is then used. When the colloidal entities are larger than several hundred nanometers, the shear rates created in the suspending fluid has more influence on the coagulation process than Brownian motion. When the coagulation process is entirely controlled by the shear rates in the flow, the term of orthokinetic (or shear) coagulation is used.

As mentioned by Owen et al. [3], coagulation/flocculation is frequently studied in batch vessels, and extensive experimental results in stirred tanks can easily be found [4–10]. However, in stirred tanks, dead volumes, inhomogeneous mixing and poor control of the local hydrodynamics can lead to unexpected coagulation issues such as fouling and broad cluster size distributions.

* Corresponding author at: Université de Toulouse, INPT, UPS, Laboratoire de Génie Chimique, 4 allée Emile Monso, F-31432 Toulouse Cedex 04, France.
E-mail address: nathalie.lesauze@iut-tlse3.fr (N. Le Sauze).

Nomenclature

A_d	aggregate diameter (m)
C	floc or aggregate strength coefficient obtained using d_{\max} (Eq. (8))
D_f	mass fractal dimension
D_{f1}	mass fractal dimension of the first class of clusters observed
D_{f2}	mass fractal dimension of the second class of clusters observed
d_{\max}	maximum aggregate diameter (m)
d_{mixer}	internal diameter of the micromixer (m)
d_{tube}	internal diameter of the tube (m)
d_i	mean diameter of class i (m)
d_{50}	50% (resp. 10%, 90%) floc diameter (m)
$G(r)$	shear rate at a distance r from the axis (s^{-1})
G_{av}	average shear rate (s^{-1})
J_{ij}	collision frequency per unit volume ($m^{-3} s^{-1}$)
k_{ij}	coagulation kernel ($m^3 s^{-1}$)
k'_{ij}	modified coagulation kernel taking efficiency into account ($m^3 s^{-1}$)
L^e	entrance length (m)
m	optical contrast
N	concentration of particles with radius r (m^{-3})
N_0	initial particle concentration (m^{-3})
N_i	concentration of particle with radius r_i (m^{-3})
p	power-law scaling exponent
q	scattering vector (m^{-1})
r	radial distance from the tube axis (m)
R	coefficient of determination
r_0	mean primary particle radius (m)
r_{tube}	internal radius of the tube (m)
Re	Reynolds number inside the reactor $((4 \cdot \rho \cdot Q) / (\mu \cdot \pi \cdot d_{\text{tube}}))$
Re_m	Reynolds number inside the mixer $((4 \cdot \rho \cdot Q) / (\mu \cdot \pi \cdot d_{\text{mixer}}))$
t	residence time (s)
$v(r)$	velocity at a distance r from the axis ($m s^{-1}$)
v_{av}	average velocity inside the tube ($m s^{-1}$)
v_{max}	maximum velocity inside the tube ($m s^{-1}$)
V_i	volume fraction of class i particles

Greek Letters

α_{ij}	collision efficiency
ϵ	dissipation rate per unit mass ($m^2 s^{-3}$)
	floc or aggregate size exponent obtained using d_{\max} (Eq. (8))
ϵ_{part}	surface energy of the particles ($J m^2$)
μ	dynamic viscosity (Pa s)
ν	kinematic fluid viscosity ($m^2 s^{-1}$)
λ	incident light wavelength (m)
ϕ	volume fraction occupied by particles
ρ	density ($kg m^{-3}$)
θ	scattering angle
ζ	zeta potential (V)

An alternative to stirred tanks is the use of tubular reactors, where local hydrodynamics are well defined in both laminar and turbulent conditions. Concerning aggregation studies in pipes with laminar flow conditions, the first studies have mainly focused on the evolution of the particle concentration over time, as well as the aggregate size distributions [11,12]. More recent studies have used laminar flow tubular reactors to study the effects of shear

flocculation processes [13] and the resulting shape of the flocs produced [14], with colloidal suspensions other than latexes.

Until now, few works have focused on the benefits of having a millimetric-scale tubular coagulator working in laminar flow conditions over both cluster size distribution and shape of the coagulated particles at aggregation equilibrium. The aim of this work is thus to further investigate coagulation of colloidal suspension inside millimetric tubes to highlight the advantages of using miniaturized equipments with laminar hydrodynamic conditions for controlled cluster size distributions (CSD) and floc shapes.

2. Theory

2.1. Shear coagulation theory

Colloidal aggregation is a long-time studied phenomenon. Almost a hundred years ago, Smoluchowski [15] theorized aggregation kinetics in analogy with chemical kinetics and proposed theoretical collision frequency expressions in the cases where particle motion is driven by Brownian motion and by laminar convection. This approach was later extended to turbulent conditions by other authors, as will be described below. In the most general case, the collision frequency per unit volume J_{ij} between two classes of particles i and j that differ by their radius r_i and r_j and present in solution at a concentration of N_i , N_j can be expressed as in Eq. (1). k_{ij} is called coagulation or aggregation kernel.

$$J_{ij} = k_{ij} \cdot N_i \cdot N_j \quad (1)$$

The expression of the coagulation kernel differs depending on the motion considered (i.e. diffusion or convection) and the hypothesis formulated by the authors.

2.1.1. Laminar coagulation

When considering shear coagulation under laminar flow, Smoluchowski [15] assumed that:

- All the collisions are efficient (i.e. there is no repulsion between the particles)
- The particles follow the fluid streamlines
- The particles are spherical

Under these assumptions, Smoluchowski [15] obtained the expression of the collision frequency per volume unit J_{ij} presented in Eq. (2), where G_{av} is the average shear rate.

$$J_{ij} = \frac{4}{3} \cdot G_{\text{av}} \cdot (r_i + r_j)^3 \cdot N_i \cdot N_j \quad (2)$$

This expression can then be implemented in a population balance to predict the evolution of the concentration of clusters of different sizes through aggregation. By considering an initially monodisperse suspension of spherical particles with a radius r_0 and concentration N , the decrease of the particle number at the very early stages is described by Eq. (3).

$$-\frac{dN}{dt} = \frac{16}{3} \cdot N^2 \cdot G_{\text{av}} \cdot r_0^3 \quad (3)$$

When the volume fraction ($\phi = 4/3 \cdot \pi \cdot r_0^3 \cdot N$) of the particles is constant through aggregation, Eq. (3) can be expressed as a pseudo first order equation (Eq. (4)).

$$-\frac{dN}{dt} = \frac{4}{\pi} \cdot \phi \cdot N \cdot G_{\text{av}} \quad (4)$$

By integrating Eq. (4), an expression giving the decrease of the number of initial particles N_0 with time can be obtained, as shown by Eq. (5) [11].

$$\frac{N}{N_0} = \exp\left(\frac{-4 \cdot \phi \cdot G_{av} \cdot t}{\pi}\right) \quad (5)$$

These expressions are well suited to extract a coagulation half-time that can be used as a qualitative description of the coagulation process [16,17]. However they cannot properly describe the cluster size evolution through the entire coagulation process.

2.1.2. Turbulent coagulation

Camp and Stein [18] demonstrated that the shear rate can be expressed in terms of dissipated energy as shown by Eq. (6).

$$G_{av} = \sqrt{\frac{\epsilon}{\nu}} \quad (6)$$

By estimating the dissipation rate per unit mass ϵ in turbulent conditions, Eq. (6) can be used to estimate G_{av} in the initial Smoluchowski equation, thereby allowing the coagulation process in turbulent conditions to be modeled. Several authors have since proposed various expressions for the turbulent coagulation rate by considering different theories. For particles under the Kolmogorov scale and using the Taylor isotropic turbulence theory, Saffman and Turner [19] obtained an expression analogous to the Camp and Stein expression. Levich [20] applied the concept of turbulent diffusion and obtained an aggregation kernel similar in structure (i.e. proportional to $G_{av} \cdot (r_i + r_j)^3$) to the previous ones, however the constant was somewhat higher (13.8 compared with 4/3). Delichatos and Probst [21] proposed an approach by using the concept of mean free path in analogy with the kinetic theory of gases. Once again their expression agrees with the structure of the previously proposed equations.

2.1.3. Collision efficiency

Smoluchowski [15] initially considered no hydrodynamic interaction between the particles. However, it is known that viscous interactions and effects induced by the particle size ratio are likely to affect the particle trajectories at small distances. This consideration has led to the use of collision efficiencies ranging between 0 and 1, which aim at correcting the conventional kernel used in the models. The corrected coagulation kernel k'_{ij} can be written as in Eq. (7), where α_{ij} is the collision efficiency.

$$k'_{ij} = \alpha_{ij} \cdot k_{ij} \quad (7)$$

In the case of homocoagulation in laminar conditions, van de ven and Mason [22] proposed an expression for collision efficiency such that the coagulation kernel is proportional to $G_{av}^{0.82}$ instead of G_{av} . Adler [23] proposed semi-empirical expressions and showed that homocoagulation is more efficient than heterocoagulation. Based on Adler's works, Han and Lawler [24] expressed the collision efficiency as being dependent on the size ratio of the approaching particles, the Hamaker constant of the material, the shear rate and the viscosity of the fluid. In addition, simplified models such as the semi-empirical efficiency model proposed by Selomulya et al. [25], which uses adjustable factors to weight the importance of the particle size ratio, have been recently proposed.

2.2. Rupture

It is conventionally accepted that in coagulation or flocculation processes, aggregation competes with the rupture of clusters or flocs [26,27]. When shear rates are high enough, the rupture phenomenon becomes preponderant. When an equilibrium state

between the aggregation and rupture processes is reached, the cluster size distribution is also in steady state. Unlike aggregation, the rupture process of aggregates has been less investigated. Nevertheless some kernel expressions have been expressed (e.g. exponential [28], power-law [29] expressions), further modified and used in population balances [25,30]. Concerning the rupture phenomenon in itself, Jarvis et al. [27] reviewed the work on floc strength and breakage and described the two main breakage mechanisms that are likely to occur:

- Surface erosion, which is a consequence of the shear stress acting tangentially on the aggregate. Small particles are removed from the surface of the aggregate, leading to an increase of polydispersity.
- Large-scale fragmentation due to tensile stress. This mechanism leads to the breakage of an aggregate into two similar size fragments.

When breakage occurs, several authors observed that the cluster size at equilibrium can be related with the average shear rate (or shear stress, as there is proportionality between these values) in the process and proposed modelings based on theoretical assumptions.

Under turbulent conditions, Parker et al. [26] observed that the evolution of the maximum aggregate diameter can be related to the shear rate following a power law, as shown by Eq. (8).

$$d_{max} = C \cdot G_{av}^{-\gamma} \quad (8)$$

d_{max} is the maximum floc or aggregate diameter, C is the floc strength coefficient and γ is the floc size exponent. C is often used as a means to assess the strength of the aggregates, and γ as an indicator of the predominant rupture mode [27]. The expression proposed by Parker was later successfully used with median floc diameters [31,32] and 95% floc diameters d_{95} [33].

More recently, Zaccone et al. [34] used mechanical considerations to formulate a correlation between the hydrodynamic stress σ undergone by clusters and the value of their gyration radius R_g at equilibrium, for very dilute suspensions, in laminar and turbulent flow conditions. The structure of the clusters is accounted for by the introduction of the mass fractal dimension D_f in the relation ($D_f = 3$ when aggregates are spherical, and less when shape deviates from sphericity). When aggregates produced are dense enough (D_f higher than 2.4), the authors proposed the following relation in laminar conditions:

$$R_g \propto \sigma^p \quad (9)$$

With p equals to $-2/(3 - D_f)[2(3.8 + 1) - \beta]$. β takes the value $-(1/3 - D_f)$ for D_f values around 2.4–2.6, and -0.4 when fractal dimension get closer to 3. The most important feature of this equation is that the scaling exponent p is directly dependent of the structure of the considered aggregate. This theoretical consideration was subsequently used in other works as a comparison basis with results either obtained by experiments [35] or numerical investigations [36,37].

Zaccone et al. also proposed an extension of Eq. (9) valid in turbulent conditions, for clusters smaller than the Kolmogorov length scale:

$$R_g \propto (\epsilon)^{-1/(3 - D_f)[2(3.8 + 1) - \eta]\delta} \quad (10)$$

δ taking into account the intermittency nature of turbulence. Comparison between experimental data and theoretical predictions of the scaling-law exponent was found to be excellent when studying coagulation of highly diluted colloidal suspension under either laminar or turbulent flow [34].

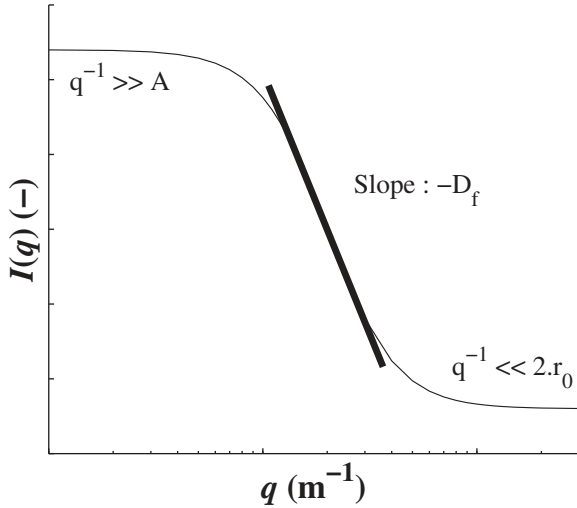


Fig. 1. Illustration of the Rayleigh-Gans-Debye approximation by plotting $I(q)$ vs. q on a Log-Log scale.

2.3. Size and morphology characterization by light scattering

Due to the complex structure of aggregates, the light scattered by these structures is somewhat more complicated to model than when only solid spheres are considered. As explained by Gregory [38], one of the most simple approaches to model the light scattered by aggregates is the Rayleigh-Gans-Debye approximation. Under the condition that the primary particles can be considered as Rayleigh scatterers (i.e. the diameter of the initial particles are much smaller than the incident wavelength λ), the structure of the aggregate is taken into account by introducing an aggregate structure factor into the expression of the scattered intensity, $I(q)$. In this case, q denotes the scattering vector which is expressed by Eq. (11), where θ is the scattering angle.

$$q = \frac{4\pi}{\lambda} \cdot \sin\left(\frac{\theta}{2}\right) \quad (11)$$

By plotting $I(q)$ as a function of q on a Log-Log scale, as demonstrated in Fig. 1, three distinct regions can be identified:

1. When $q^{-1} \gg A_d$, the characteristic size of an aggregate, scattering depends essentially on the squared volume of particles within the agglomerate, and is thus independent of the aggregate shape.
2. When $q^{-1} \ll 2 \cdot r_0$, i.e. the diameter of the initial particles, the intensity of the scattered light is not influenced by the particle structure; the light scattered by a n -particle aggregate is the same as the light scattered by n initial particles.
3. For intermediates q values, $I(q) \propto q^{-D_f}$. In this particular region, information about the shape of the aggregate can be thus extracted using light scattering data of the measured samples by assuming the Rayleigh-Gans-Debye approximation.

When the aggregate shapes deviate from sphericity, the raw light intensity data is used to obtain the mean mass fractal dimension of the samples. It allows then to estimate a global aggregate shape [38].

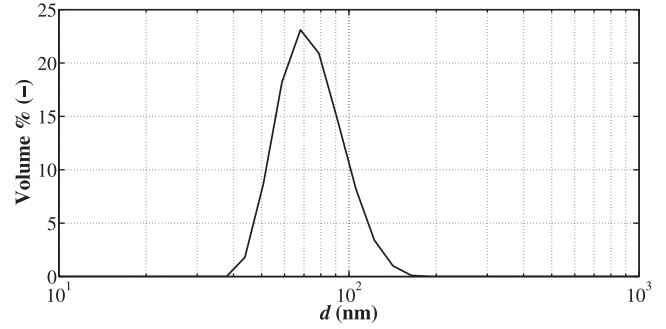


Fig. 2. Particle size distribution of the initial latex obtained with Nanosizer ZS®.

3. Material and methods

3.1. Materials

3.1.1. Latex

The latex studied is a core-shell PMMA/PABu copolymer, stabilized by a carboxylic acid surfactant. The experiments are carried out using 1% (w/w) concentrated latex, which is obtained after diluting an initial suspension (33%, w/w) using ultrapure water (Purelab® Option-Q). After mixing with the coagulant, the concentration of the flowing suspension is 0.5% (w/w) (corresponding to $\phi = 0.0046$). Working with such a moderate concentration allows the obtention of steady state cluster size distribution within a few seconds at moderate shear rates. Prior to the destabilization experiments, particle size distribution and zeta potential of the initial suspension are determined using a Malvern Nanosizer ZS®. Three measurements are performed to check the stability and the size distribution of the initial product. The volume-averaged diameter of the latex is 82 nm. The polydispersity index PDI is 0.037, which indicates a narrow initial size distribution since the PDI value is below 0.05. This is confirmed by the particle size distribution measurement shown in Fig. 2. The average value of zeta potential is $\zeta = -63.8$ mV. A colloidal suspension is usually considered stable if $|\zeta| > 30$ mV, thus the value obtained meets this stability criterion.

3.1.2. Coagulant

The pKa of carboxylic acids is usually in the range between 4 and 5. Using a sufficient amount of concentrated sulfuric acid is thus an efficient way to ensure that no charges remain at the particle surface and to avoid ineffective aggregation induced by electrostatic repulsions. In the following experiments, coagulation is carried out using H_2SO_4 with concentration of 0.02 mol L^{-1} . Since off-line analyses are carried out, the samples are quenched in diluted solution of NaOH to ensure the stability of the suspension before analysis.

3.2. Pilot set-up design

Fouling is a main issue when using suspensions, especially inside the motion device where the suspension is likely to undergo high shear rates (e.g. inside a pump head). The set-up presented in Fig. 3 is designed to avoid direct contact between the motion system and the fluid. A commercial pressure system (A) (FLUIGENT MFCS™-EZ pressure controller, 4 channels) is used to create fluid flow; pressure is the main driving force in the system, thereby involving no direct contact between the device and the suspension.

Four stainless steel tanks (1L capacity) are used as storage tanks (B). The first tank contains the latex and the third tank holds the coagulant (sulfuric acid). The second and fourth tanks are used to store water and rinse the system after each experiment. The outlet tube of each tank is connected to a 3-way valve, which enables easy switching between the main fluid and rinsing water. The flow

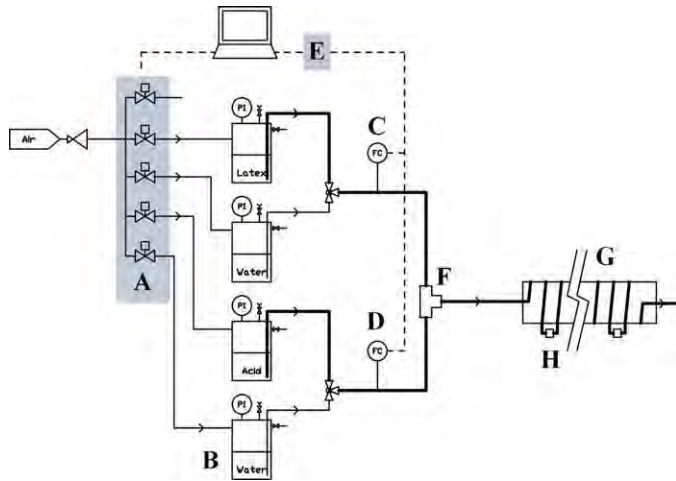


Fig. 3. Experimental millifluidic set-up.

Table 1
Properties of the reactors used for the experiments.

Reactor	Internal diameter (mm)	Total length (m)	Material
1	1.57	16.0	PFA
2	2.00	10.2	PTFE
3	2.40	12.2	ETFE

rates are measured and regulated by two calorimetric flow meters (FLUIGENT Flow Unit XL) (C, D), which are connected to a management platform (FLUIGENT Flowboard) (E) communicating with a computer.

The outlets of the flow meters are linked to a T-mixer (internal diameter $d_{\text{mixer}} = 1.27$ mm) (F), which allows fast mixing of the reactants at moderate Reynolds numbers (around 400 in this study). The flow rate conditions are fixed at $Q_{\text{acid}} = Q_{\text{latex}} = 0.5 \times Q$, where Q is the total flow rate inside the tube. Then, the coagulating solution is introduced into the milli-tube reactor, which is wound around an 8 cm diameter stainless steel support (G). As the diameter of the support is much greater than the internal diameter of the tube (2.4 mm or less), no significant centrifugal effects or Dean vortices are expected with this set-up.

3.3. Characteristics of the tubular reactors

The millireactors consist in fluoropolymer capillaries. In order to broaden the range of average shear rate studied, three tubings with different internal diameters are used. The interest of such materials is to avoid fouling on the inner wall and to resist to corrosion. The properties of the tubular reactors are listed in Table 1.

Each reactor is divided into eight equal lengths in order to observe, in an appropriate latex concentration range, the CSD evolution as a function of residence time and to quantify the length and time needed to reach the clusters equilibrium size. The connection between each length is ensured using flangeless 1/8" fittings (H in Fig. 3); these can be unscrewed during the experiment to take samples. The internal diameter of the feeding tubes is 0.5 mm, which is much smaller than the diameter of the tubular reactor ones. As a result, the pressure loss across the system is mostly due to circulation inside the feeding tubes, and therefore the flow is not disturbed when the fittings are unscrewed for sampling. This set-up is also very flexible and easily allows the reactor length to be increased if needed.

3.4. Hydrodynamics

As reactants used in the study are diluted enough, the mixture properties considered for calculations are those of the continuous phase (ultrapure water) at operating conditions ($\rho = 1000 \text{ kg m}^{-3}$, $\mu = 10^{-3} \text{ Pa s}$, Newtonian and incompressible fluid). Using these properties, an estimation of the needed entrance length L^e considering laminar flow in smooth channel can be calculated using Eq. (12) [39–41].

$$\frac{L^e}{d_{\text{tube}} \cdot Re} = 0.1 \quad (12)$$

For this study, the maximal entrance length calculated is 7.5 cm (Reactor 2, $Re = 373$) and lower than the tube length needed to perform the first sample (1.275 m for Reactor 2): the establishment of laminar flow is thus guaranteed for all cases. In laminar established flow conditions, assuming that the fluid is both incompressible and Newtonian, the velocity inside a tube with a circular cross-section obeys the well-known Poiseuille law. This gives a parabolic velocity profile as a function of the radial distance from the tube centerline as given in Eq. (13), where r_{tube} is the internal radius of the tube, and v_{max} the maximum velocity at the tube centerline.

$$v(r) = v_{\text{max}} \cdot \left(1 - \left(\frac{r}{r_{\text{tube}}}\right)^2\right) \quad (13)$$

The first derivative of the velocity profile provides an expression for the shear rate at a radial distance r (Eq. (14)).

$$G(r) = \left| \frac{dv(r)}{dr} \right| = \frac{2 \cdot v_{\text{max}} \cdot r}{r_{\text{tube}}^2} \quad (14)$$

Thus the shear rate is linearly proportional to the radial distance and the following boundary conditions exist:

- The velocity is maximal and the shear rate is zero at the centerline of the tube ($r = 0$);
- The velocity is zero and the shear rate is maximal at the tube walls ($r = r_{\text{tube}}$).

Since the shear rate varies over the radius of the tube an average shear rate is determined following Eq. (15).

$$G_{\text{av}} = \frac{\int_0^{r_{\text{tube}}} G(r) \cdot 2 \cdot \pi \cdot r \cdot dr}{\int_0^{r_{\text{tube}}} 2 \cdot \pi \cdot r \cdot dr} = \frac{4 \cdot v_{\text{max}}}{3 \cdot r_{\text{tube}}} \quad (15)$$

3.5. Light scattering analysis

Light scattering analyses of the suspension are performed using a Malvern Mastersizer 2000[®] and liquid dispersion unit HydroS[®] (1400 RPM) in order to determine the cluster size distribution of the samples. Each sample is analyzed three times to check stability during the analysis. Excellent sample stability is found in all cases. The refractive index and the absorption index of the latex are 1.59 and zero, respectively.

4. Experiments and results

4.1. Mixing and flow properties

Prior experiments highlighted the necessity of a good mixing between both reactants to avoid plugging issues due to fast aggregation process. Numerous studies [42–46] have shown that fast mixing (in the range of few milliseconds) can be achieved in T-mixers. Indeed, at Reynolds numbers (Re) greater than 400, vortices are created at the T-junction which enhances mixing. To ensure good mixing quality in the T-mixer used (internal diameter

Table 2
Flow properties in the experiments.

Reactor	Q (mL min ⁻¹)	v _{av} (m s ⁻¹)	Re (-)	Re _m (-)	G _{av} (s ⁻¹)
3	24.0	0.09	212	401	197
3	29.4	0.11	260	491	241
3	34.0	0.13	301	568	278
2	24.0	0.13	255	401	340
2	28.0	0.15	297	468	396
2	35.1	0.19	373	586	497
1	24.0	0.21	324	401	702
1	34.0	0.29	460	568	994

Table 3
Evolution of the span, uniformity and median volume diameter d_{50} of the cluster size distribution with residence time for $G_{av} = 497 \text{ s}^{-1}$.

Sample	Residence time (s)	Span (-)	Uniformity (-)	d_{50} (μm)
1	7	1.14	0.36	153
2	17	1.16	0.37	166
3	21	1.24	0.39	124
4	27	1.15	0.37	146
5	34	1.15	0.36	142
6	41	1.19	0.38	157
7	48	1.17	0.37	160
8	55	1.15	0.36	153
Average	-	1.17	0.37	150

$d_{\text{mixer}} = 1.27 \text{ mm}$), the flow rates have been chosen such that the Reynolds number in the mixer (Re_m) is greater than 400. Table 2 lists the flow rates investigated in reactors 1, 2, 3, as well as the average fluid velocities, Reynolds numbers and the resulting average shear rates.

4.2. Cluster size distribution results

4.2.1. Properties measured

The volume median diameter of the distribution (d_{50}) is determined for each experiment. Uniformity is proposed as a measurement of the absolute deviation from the median (Eq. (16)).

$$\text{Uniformity} = \frac{\sum V_i |d_{50} - d_i|}{d_{50} \cdot V_i} \quad (16)$$

where d_i is the mean diameter of class i clusters and V_i their volume fraction.

The span of a distribution, presented in Eq. (17), gives an information about the width of the distribution measured. d_{10} is the 10% aggregate diameter.

$$\text{Span} = \frac{d_{90} - d_{10}}{d_{50}} \quad (17)$$

4.2.2. Evolution of the properties as a function of residence time

Cluster size distributions are measured for all experiments at eight locations along the tube, corresponding to eight different residence times. For all conditions studied, it appears that aggregation process is very fast, which confirms the importance of a good mixing between the reactants. Indeed, for a given experiment, the observed parameters (span, uniformity and characteristic diameters) are roughly the same at each sampling point. This means that in the experimental conditions imposed -i.e. fast mixing, shear rates and latex concentration- particle aggregation steady state is achieved before the first sampling point. As an example, Table 3 shows the results for the experiment at $G_{av} = 497 \text{ s}^{-1}$ (reactor 2, $Q = 35.1 \text{ mL min}^{-1}$) and Fig. 4 presents cluster size distributions observed at $G_{av} = 497 \text{ s}^{-1}$ and $t = 7 \text{ s}$, 21 s, 48 s.

This methodology allows information on the polydispersity and the shape of the aggregates to be obtained as a function of shear rate. For that purpose, an average of the different size characteristics

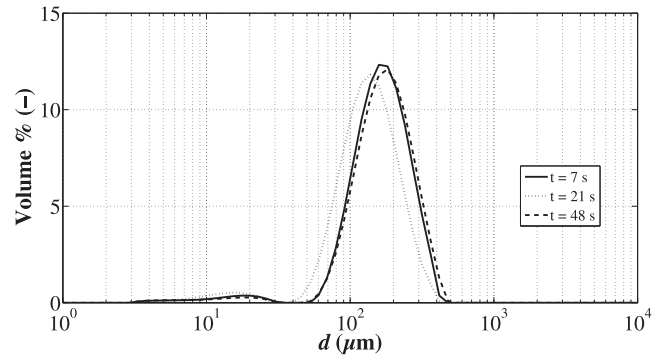


Fig. 4. CSD of the coagulated latex at $G_{av} = 497 \text{ s}^{-1}$ and $t = 7 \text{ s}$, 21 s, 48 s.

Table 4
Averaged span, uniformity and d_{50} at the studied average shear rates.

G_{av} (s ⁻¹)	Span (-)	Uniformity (-)	d_{50} (μm)
197	2.01	0.62	327
241	2.02	0.62	306
278	1.45	0.45	241
340	1.30	0.41	230
396	1.45	0.45	229
497	1.17	0.37	150
702	1.21	0.38	165
994	1.30	0.42	107

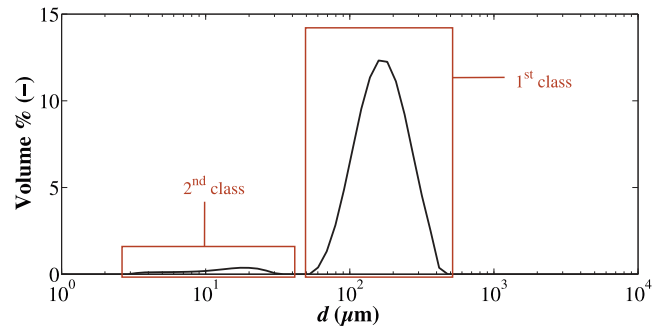


Fig. 5. Distinction between two classes of particles.

measured at the eight samples is calculated, allowing a more accurate quantification. By lowering the initial particle concentration, some dynamics can possibly be observed. However, as the main purpose of the study is to observe the clusters size and shape properties at aggregation/breakage equilibrium, these considerations will be the ground basis for a subsequent work.

4.2.3. Influence of the shear rate

The average values obtained for the span, uniformity and d_{50} at the different shear rates studied are presented in Table 4.

It can be seen that the span and the uniformity tend to decrease with an increasing average shear rate until the value $G_{av} = 497 \text{ s}^{-1}$, and present few evolution beyond that value. This implies that the polydispersity of the sample decreases with increasing shear rate until reaching a plateau. This information is important for processes aimed at producing aggregates at a calibrated size and quality. Also, a decrease of d_{50} is observed when increasing average shear rate, indicating that at these operating conditions, rupture plays a significant role in the equilibrium state observed.

Another interesting result is highlighted in Fig. 5. Two classes of cluster size distributions can be distinguished: a main peak, labeled 1st class, and another class (2nd class). The latter is almost insignificant volume-wise and thus unlikely to have huge influence on the cluster size distribution properties shown in Table 4.

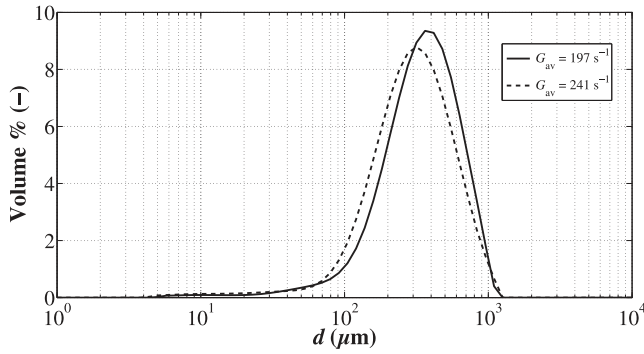


Fig. 6. Behavior of the CSD at $G_{av} = 197 \text{ s}^{-1}$ and 241 s^{-1} .

Table 5

Evolution of the volume percentage of the 2nd class with average shear rate.

$G_{av} (\text{s}^{-1})$	Volume % (-)
994	5.2
702	3.2
497	3.4
396	2.8
340	2.1
278	2.2
241	0.0
197	0.0

Two possible reasons may explain the existence of the 2nd class:

- The non-homogeneous shear rate across the cross section of the tube. As no significant Dean vortices are expected inside the tube, high polydispersity could result from faster aggregation at the walls (where the shear rate is maximal) than near the tube center (where the shear rate is minimal).
- The rupture of the largest aggregates, to form smaller ones. Large-scale fragmentation is thought to form two similar broken flocs and thus unlikely to explain this behavior. As described in the theoretical part, erosion is likely to promote the appearance of small aggregates, which are broken from the surface of the largest particles. In a laminar flow reactor, viscous dissipation is responsible for energy dissipation throughout the reactor. This viscous dissipation induces tangential stress that can be responsible for erosion of the largest aggregates.

In the shear rate range studied, the rupture of aggregates is expected to occur. One way to assess the influence of rupture on the presence of these particles is to calculate the cumulated volume percentage of the sample represented by the 2nd class. If the particles in the 2nd class are mostly due to poor aggregation, an increase of the shear rate should reduce the volume percentage within this class. On the other hand, if they are mainly a result of surface erosion, an increased shear rate will increase the stress undergone by the aggregates, thereby breaking more particles from the surface.

For the experiments led at $G_{av} = 197$ and 241 s^{-1} (low shear rate), the shape of the CSD observed is presented in Fig. 6. Two classes of particles are not distinguished at these shear rate conditions; this means that no information about erosion can be deduced from these two experiments.

As shown in Table 5, a volume percentage of the 2nd class is only distinguished for shear rates $G_{av} = 278 \text{ s}^{-1}$ and greater.

The global trend observed in Table 5 is an increase of the volume % of cluster size in the 2nd class with an increase of the shear rate. This observation suggests that rupture plays a major role in the formation of these smaller particles and that erosion has a significant effect on the cluster size distribution in this type of system.

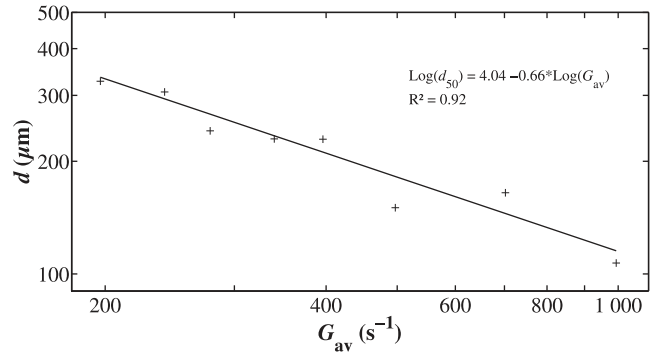


Fig. 7. Evolution of d_{50} vs. G_{av} (Log-Log scale).

4.3. Cluster breakup modeling

4.3.1. Scaling of the median cluster diameter with shear rate

When breakup have a significant impact on the cluster size distribution, it is well known that the steady-state diameter of the clusters will decrease with increasing shear rate. To observe this trend, the median cluster diameter at steady state was plotted versus the average shear rate inside the reactor.

The Log-Log representation presented in Fig. 7 shows that the results can be reasonably modeled ($R^2 = 0.92$) with a power law of scaling exponent -0.66 .

4.3.2. Comparison with the modeling approaches proposed in the literature

The scaling exponent derived from the experimental results obtained can be compared to the predictions proposed by Parker and Zaccone, also modeling the decrease of the cluster size with increasing shear rate using a power law.

The approach proposed by Parker directly relates the scaling exponent with the main breakage mechanism occurring in the process. When viscous dissipations are involved, following Parker theory, an exponent equals to -0.5 indicates that fragmentation is the main degradation mode, whereas when the exponent equals -1 , erosion is. Although the study led by Parker is strictly valid in turbulent conditions, it is well-known that in the smallest eddies of turbulence, an analogy can be formulated between viscous dissipation in laminar conditions (induced by the friction between molecules and dissipated tangentially to the fluid motion) with energy dissipation in turbulent conditions that results from the motion of turbulent eddies, inducing tangential stress. Several studies even go further by writing that in the smallest eddies, the flow behaves like laminar. Therefore it appears reasonable to use these exponent values, obtained by Parker for clusters smaller than the Kolmogorov length scale, as guidelines for interpreting the degradation mode in the experiments. The value obtained here (-0.66) suggests the contribution of both rupture mechanisms to the particle degradation, and agrees with the results of the volume percentage of the second class. Indeed, fragmentation generates relatively large particles, which will not contribute to the second class of particles and thus cannot be detected with volume percentage data in Table 5.

Alternatively, Zaccone et al. proposed a model based on mechanical considerations and also deduced a power law dependency between the aggregate size and the average shear rate. As reported before, the scaling exponent p obtained by Zaccone et al. is directly dependent of the structure of the aggregates considered. Some information about mass fractal dimension of the samples measured has thus to be obtained to quantify this dependency.

As the diameter of the primary particles is smaller than the laser wavelength of the analytical device, the Rayleigh-Gans-Debye

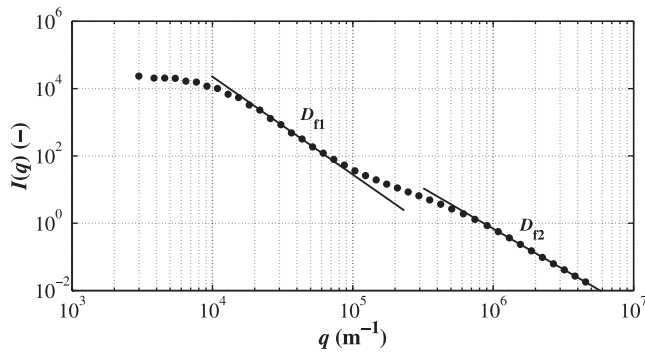


Fig. 8. Experimental light scattering raw data ($G_{av} = 396 \text{ s}^{-1}$), 5th sample.

Table 6
Mass fractal dimensions D_{f1} and D_{f2} extracted from the raw light scattering data.

$G_{av} (\text{s}^{-1})$	$D_{f1} (-)$	$D_{f2} (-)$
197	2.45	2.29
241	2.51	2.38
278	2.66	2.40
340	2.67	2.42
396	2.68	2.48
497	2.67	2.56
702	2.68	2.45
994	2.66	2.54

theory can be used to extract mass fractal dimension values. A $I(q)$ vs. q plot (in Log-Log scale) of light scattering data obtained is presented Fig. 8 ($G_{av} = 396 \text{ s}^{-1}$, sample point 5). As we can see, two distinct linear regions can be distinguished, at low q values and at large q values. As presented earlier, the CSD results exhibit two distinct particle classes that can be related to these two slopes. According to Mie theory, the largest aggregates strongly scatter light at low q values. D_{f1} can thus be interpreted as the mean fractal dimension of the first class of particles. The fractal dimension D_{f2} is extracted at high q values, where the intensity measured is strongly influenced by the scattering of the smallest aggregates. D_{f2} can then be assimilated to the mean fractal dimension of aggregates included in the second class identified earlier. The average values collected for D_{f1} and D_{f2} are shown in Table 6.

Interestingly, the fractal dimension of the smallest aggregates, D_{f2} , keeps increasing as the average shear rate increases (between 2.3 and 2.6) whereas D_{f1} can be considered as steady (around 2.68) starting $G_{av} = 278 \text{ s}^{-1}$. Such high values are commonly observed for aggregates generated by laminar flow [34,35,47,48]. As explained by several authors [1,34], the collision mode generated by a laminar flow is ballistic, meaning a combination of ballistic cluster-cluster and particle-cluster aggregation. Theoretically, if the flow induces ballistic particle-cluster aggregation, fractal dimensions up to 3 can be obtained. Ballistic cluster-cluster aggregation will generate clusters with fractal dimension somewhat lower (around 2). In laminar flow, ballistic particle-cluster is supposed to be the predominant collision mode. However, as the flow penetrates through the aggregates, deviations from the theory are observed [49], explaining the obtention of D_f values higher than 2, however lower than 3. Furthermore, the fractal dimension of the smallest aggregates is always smaller than the one of the largest. Such behavior can be explained by the influence of recombination on larger aggregates, known to gives more compact aggregates [50–52]. Also, selective breakage of the weakest parts of the clusters occurring at high shear rates will lead to denser structures [47,48]. The combination of these effects thus explains the difference observed between D_{f1} and D_{f2} .

For Zaccone et al., the power-law exponent p depends on the fractal dimension value. When considering breakage in such a poly-disperse suspension, only the largest aggregates (meaning the first

class of particles) are expected to be affected by breakage. Only D_{f1} is then considered for interpreting results. As D_{f1} quickly reach a steady-state value (2.68), this value is used in Eq. (9), taking β equal to -0.4 (as D_{f1} is close to 3) to estimate p . The calculation gives $p = -0.63$ and is thus in excellent agreement with the experimental results obtained.

It is worth noting that for such a volume concentration ($\phi = 0.0046$), an other explanation could be discussed. At moderate volume concentration ($\phi = 0.05$), Kroupa et al. [37] observed discrepancies with Zaccone approach. The authors explain that for this concentration value, not only rupture but also aggregation will have an impact on equilibrium. In that case, Kroupa et al. suggest that cluster size will then be highly influenced by the balance between the hydrodynamic force acting on the cluster and the adhesive forces between primary particles. By expressing a straightforward balance between these forces, the authors proposed the cluster mean diameter to be proportional to $G_{av}^{-0.5}$. While performing numerical DEM investigation on the size and structure of aggregates formed under laminar flow, Kroupa et al. observed a scaling exponent equal to -0.65 , and thus close to their theoretical predictions and very close to the scaling exponent here observed.

5. Conclusion

Acrylic latex coagulation with concentrated sulfuric acid in millireactors under laminar flow conditions has been investigated. A pseudo steady-state was observed quickly, resulting from a balance between aggregation and rupture phenomena. As the average shear rate increased, a second population of cluster sizes was observed in the cluster size distributions despite a global decrease of the volume distribution width. This is believed to be due mainly to the presence of surface erosion induced by viscous dissipation. The volume median diameter d_{50} was found to follow a power law with shear rate, with a scaling exponent equal to -0.66 . The value of the exponent was compared with theoretical calculations suggested by Zaccone et al., and found to be in very good agreement. The combination of laminar flow, inducing ballistic collision, with the effects of shear rate on particle structure allows high fractal dimension values, and therefore more spherical aggregates to be obtained. The use of laminar flow millireactors for coagulation-flocculation processes therefore appears to be of great interest for controlling cluster size. Indeed, despite the laminar conditions, high shear rates can be achieved, thereby promoting controlled aggregate size and shape, which are of interest in diverse process industries.

Acknowledgment

This work was supported by the French National Research Agency (ANR), in the framework of the Scale-Up project (ANR-12-RMNP-0016).

References

- [1] E. Carissimi, J. Rubio, The flocs generator reactor – FGR: a new basis for flocculation and solid-liquid separation, *Int. J. Miner. Process.* 75 (February (3–4)) (2005) 237–247.
- [2] N. Furukawa, W. Okada, Analysis of the coagulation rate of MBS (methylmetacrylate-butadiene-styrene) polymer latex and strength of coagula, *Adv. Powder Technol.* 5 (2) (1994) 161–175.
- [3] A.T. Owen, P.D. Fawell, J.D. Swift, D.M. Labbett, F.A. Benn, J.B. Farrow, Using turbulent pipe flow to study the factors affecting polymer-bridging flocculation of mineral systems, *Int. J. Miner. Process.* 87 (3–4) (2008) 90–99.
- [4] G.B.J. De Boer, G.F.M. Hoedemakers, D. Thoenes, Coagulation in turbulent flow: part I, *Inst. Chem. Eng.* 67 (1989) 301–307.
- [5] Y. Li, G. Xu, M. Chen, K. Wang, Slow pelleting coagulation of MBS latex, *Chem. Eng. Res. Des.* 75 (Part A) (1997).
- [6] G.B.J. De Boer, C. De Weerd, D. Thoenes, Coagulation in turbulent flow: part II, *Inst. Chem. Eng.* 67 (1989) 308–315.

- [7] P.T.L. Koh, J.R.G. Andrews, P.H.T. Uhlherr, Flocculation in stirred tanks, *Chem. Eng. Sci.* 39 (6) (1984) 975–985.
- [8] M. Kobayashi, T. Maekita, Y. Adachi, H. Sasaki, Colloid stability and coagulation rate of polystyrene latex particles in a turbulent flow, *Int. J. Miner. Process.* 73 (2–4) (2004) 177–181.
- [9] J. Gregory, Polymer adsorption and flocculation in sheared suspensions, *Colloids Surf.* 31 (1988) 231–253.
- [10] M. Soos, A.S. Moussa, L. Ehrh, J. Sefcik, H. Wu, M. Morbidelli, Effect of shear rate on aggregate size and morphology investigated under turbulent conditions in stirred tank, *J. Colloid Interface Sci.* 319 (2) (2008) 577–589.
- [11] J. Gregory, Flocculation in laminar tube flow, *Chem. Eng. Sci.* 36 (11) (1981) 1789–1794.
- [12] K. Higashitani, S. Miyafusa, T. Matsuda, Y. Matsuno, Axial change of total particle concentration in Poiseuille flow, *J. Colloid Interface Sci.* 77 (1) (1980) 21–28.
- [13] I.C. Tse, K. Swetland, M.L. Weber-Shirk, L.W. Lion, Fluid shear influences on the performance of hydraulic flocculation systems, *Water Res.* 45 (17) (2011) 5412–5418.
- [14] F. Vaezi G., R.S. Sanders, J.H. Masliyah, Flocculation kinetics and aggregate structure of kaolin mixtures in laminar tube flow, *J. Colloid Interface Sci.* 355 (1) (2011) 96–105.
- [15] M. Smoluchowski, Drei vorträge über diffusion, Brownsche molekularbewegung und koagulation von kolloidteilchen, *Phys. Z. Sowjetunion* 17 (1916) 557–599.
- [16] F.E. Torres, W.B. Russel, W.R. Schowalter, Flocc structure and growth kinetics for rapid shear coagulation of polystyrene colloids, *J. Colloid Interface Sci.* 142 (2) (1991) 554–574.
- [17] L.G.B. Bremer, P. Walstra, T. van Vliet, Estimations of the aggregation time of various colloidal systems, *Colloids Surf. A: Physicochem. Eng. Aspects* 99 (2–3) (1995) 121–127.
- [18] T.R. Camp, P.C. Stein, Velocity Gradients and Internal Work in Fluid Motion, (Massachusetts Institute of Technology. Dept. of Civil Engineering). MIT, 1943 (bibtext: camp1943velocity).
- [19] P.G. Saffman, J.S. Turner, On the collision of drops in turbulent clouds, *J. Fluid Mech.* 1 (01) (1956) 16–30.
- [20] V.G. Levich, *Physicochemical Hydrodynamics*, Englewoods Cliffs, Prentice-Hall, 1962.
- [21] M.A. Delichatsios, R.F. Probstein, Coagulation in turbulent flow: theory and experiment, *J. Colloid Interface Sci.* 51 (3) (1975) 394–405.
- [22] T.G.M. van de Ven, S.G. Mason, The microrheology of colloidal dispersions VII. Orthokinetic doublet formation of spheres, *Colloid. Polym. Sci.* (255) (1977) 468–479.
- [23] P.M. Adler, Heterocoagulation in shear flow, *J. Colloid Interface Sci.* 83 (1) (1981) 106–115.
- [24] M. Han, D. Lawler, The (relative) insignificance of G in flocculation, *J. AWWA* 84 (10) (1992) 79–91.
- [25] C. Selomulya, G. Bushell, R. Amal, T.D. Waite, Understanding the role of restructuring in flocculation: the application of a population balance model, *Chem. Eng. Sci.* 58 (2) (2003) 327–338.
- [26] D.S. Parker, W.J. Kaufman, D. Jenkins, Flocc breakup in turbulent processes, *J. Sanit. Eng. Div.* 98 (1) (1972) 79–99.
- [27] P. Jarvis, B. Jefferson, J. Gregory, S.A. Parsons, A review of floc strength and breakage, *Water Res.* 39 (14) (2005) 3121–3137.
- [28] M.A. Delichatsios, R.F. Probstein, The effect of coalescence on the average drop size in liquid–liquid dispersions, *Ind. Eng. Chem. Fundam.* 15 (2) (1976) 134–138.
- [29] K.J. Valentas, O. Bilous, N.R. Amundson, Analysis of breakage in dispersed phase systems, *Ind. Eng. Chem. Fundam.* 5 (2) (1966) 271–279.
- [30] P. Somasundaran, V. Runkana, Modeling flocculation of colloidal mineral suspensions using population balances, *Int. J. Miner. Process.* 72 (1–4) (2003) 33–55.
- [31] R.J. François, Strength of aluminium hydroxide flocs, *Water Res.* 21 (9) (1987) 1023–1030.
- [32] J. Leentvaar, M. Rebhun, Strength of ferric hydroxide flocs, *Water Res.* 17 (8) (1983) 895–902.
- [33] D.H. Bache, E. Rasool, D. Moffat, F.J. McGilligan, On the strength and character of alumino-humic flocs, *Water Sci. Technol.* 40 (9) (1999) 81–88.
- [34] A. Zaccone, M. Soos, M. Lattuada, H. Wu, M.U. Bäbler, M. Morbidelli, Breakup of dense colloidal aggregates under hydrodynamic stresses, *Phys. Rev. E* 79 (June 6) (2009).
- [35] M. Soos, L. Ehrh, M.U. Bäbler, M. Morbidelli, Aggregate breakup in a contracting nozzle, *Langmuir* 26 (1) (2010 January) 10–18.
- [36] Y.M. Harshe, M. Lattuada, Breakage rate of colloidal aggregates in shear flow through Stokesian dynamics, *Langmuir* 28 (January 1) (2012) 283–292.
- [37] M. Kroupa, M. Vonka, M. Soos, J. Kosek, Size and structure of clusters formed by shear induced coagulation: modeling by discrete element method, *Langmuir* 31 (28) (2015) 7727–7737.
- [38] J. Gregory, Monitoring particle aggregation processes, *Adv. Colloid Interface Sci.* 147–148 (2009) 109–123.
- [39] P. Gao, S. Le Person, M. Favre-Marinet, Scale effects on hydrodynamics and heat transfer in two-dimensional mini and microchannels, *Int. J. Therm. Sci.* 41 (11) (2002) 1017–1027 (bibtext: Gao20021017).
- [40] S. Shen, J.L. Xu, J.J. Zhou, Y. Chen, Flow and heat transfer in microchannels with rough wall surface, *Energy Convers. Manage.* 47 (11–12) (2006) 1311–1325.
- [41] N. Di Miceli Raimondi, L. Prat, C. Gourdon, J. Tasselli, Experiments of mass transfer with liquid–liquid slug flow in square microchannels, *Chem. Eng. Sci.* 105 (2014) 169–178.
- [42] N. Kockmann, C. Foll, P. Woias, Flow regimes and mass transfer characteristics in static micromixers, *Proc. SPIE* 4982 (2003) 319–329.
- [43] S. Wong, M. Ward, C. Wharton, Micro T-mixer as a rapid mixing micromixer, *Sens. Actuators B: Chem.* 100 (3) (2004) 359–379.
- [44] M. Engler, N. Kockmann, T. Kiefer, P. Woias, Numerical and experimental investigations on liquid mixing in static micromixers, *Chem. Eng. J.* 101 (1–3) (2004) 315–322.
- [45] M. Hoffmann, Michael Schluter, Norbert Rabiger, Experimental investigation of liquid–liquid mixing in T-shaped micro-mixers using -LIF and -PIV, *Chem. Eng. Sci.* 61 (9) (2006) 2968–2976.
- [46] B. Palanisamy, B. Paul, Continuous flow synthesis of ceria nanoparticles using static T-mixers, *Chem. Eng. Sci.* 78 (2012) 46–52.
- [47] V. Oles, Shear-induced aggregation and breakup of polystyrene latex particles, *J. Colloid Interface Sci.* 154 (2) (1992) 351–358.
- [48] J.L. Burns, Y. Yan, G.J. Jameson, S. Biggs, A light scattering study of the fractal aggregation behavior of a model colloidal system, *Langmuir* 13 (24) (1997) 6413–6420.
- [49] P.B. Warren, R.C. Ball, A. Boelle, Convection-limited aggregation, *EPL (Europhys. Lett.)* 29 (4) (1995) 339.
- [50] C. Selomulya, R. Amal, G. Bushell, T.D. Waite, Evidence of shear rate dependence on restructuring and breakup of latex aggregates, *J. Colloid Interface Sci.* 236 (1) (2001) 67–77.
- [51] P.T. Spicer, S.E. Pratsinis, Shear-induced flocculation: the evolution of floc structure and shape of the size distribution at steady state, *Water Res.* 30 (5) (1996) 1049–1056.
- [52] A. Yeung, A. Gibbs, R. Pelton, Effect of shear on the strength of polymer-induced flocs, *J. Colloid Interface Sci.* 196 (1) (1997) 113–115.